

CFD ANALYSIS FOR THE EXPERIMENTAL INVESTIGATION OF A SINGLE CHANNEL POST-BLOWDOWN

Hyung Seok Kang

Korea Atomic Energy Research Institute, Korea

Abstract

A CFD (Computational Fluid Dynamics) benchmark calculation for the steady state phase of the post-blowdown experiment in a single high fuel channel was performed to assist in the development of an accident analysis program for CANDU-6 at KAERI. The CFD results showed a good agreement with the test data as whole. However, the CFD results overestimated the temperature of the pressure tube. This means that the calculated thermal resistance through the annulus gap between the pressure tube and the calandria tube in the CFD analysis is high when compared to the test data. If the proper gas absorption coefficient of CO₂ is chosen for the radiation transport equation through the annulus gap, better CFD results will be generated.

Introduction

In the previous LBLOCA (Large Break Loss Of Coolant Accident) analysis methodology adopted for Wolsong 2, 3, and 4's licensing, the fuel channel blowdown phase was analyzed by a CANDU system analysis code CATHENA, an advanced two-fluid thermal hydraulic code, and the post-blowdown phase of a fuel channel was analyzed by the CHAN-IIA code [1-3]. The blowdown and post-blowdown phases in the LBLOCA were defined at before and after 40 seconds when the pressure of the fuel channel was depressurized to about an atmospheric pressure. The main concern of a fuel channel analysis for the blowdown and post-blowdown phases is a radiative heat transfer from the hot fuel bundle under an insufficient steam flow to the cold moderator to keep fuel temperature below the threshold of the self-catalytic exothermic metal-water reaction of the fuel under long term decay heat conditions [3-6]. Pressure tube ballooning contact with the calandria tube resulting in a dryout of the outside calandria tube can lead to a fuel channel rupture [3,4].

A refined analysis tool that can accomodate the complicated multi-dimensional thermal hydraulic behavior in the fuel channel needs to be developed in order to answer these two important safety issues. These phenomena are expected to be highly multi-dimensional, being dependent on the complicated geometry of the fuel channel, especially for a combined radiation and convective heat transfer between the heat structures and the steam flow [2-4]. The multi-dimensional phenomena inside the cluster type of the CANDU fuel bundle has been simulated for the post-blowdown event to consider the complicated geometry and heat transfer in the fuel channel after recent Wolsong 2, 3, 4 licensing studies by using the CATHENA code [3,4]. This was mainly due to its superiority over CHAN-IIA in the modeling capability of the heat transfer in the complicated fuel channel geometries and the flexibility of dealing with the complex network of the hydrodynamic nodes [2-4,7].

The use of one computer code in consecutive analyses appeared to be desirable for a consistency and simplicity in the safety analysis process [2,3]. However, validation of the high temperature post-blowdown fuel channel model in the CATHENA before being used in the accident analysis is necessary. Experimental data for the 37-element fuel bundle that fuels CANDU-6 has not been performed [5,6,8-10]. The benchmark problems for the 37-element fuel bundle by using the CFD code was compared with the test results of the 28-element fuel bundle in the CS28-1 experiment. The CS28-1 test examined the fuel heat-up phenomena and metal-water exothermic reaction phenomena of the fuel and radiative heat transfer phenomena between the fuel, and the pressure and calandria tubes under high temperature conditions [5,6,8-10]. A detailed evaluation of the test data, and a multidimensional simulation of the test section by the CFD code, CFX5.7, is required to better understand this simulated event [3,11-13]. And also, the CFD code will be used to verify the post-blowdown model of the CATHENA for a 37-element fuel bundle.

Post-Blowdown Experiment

The CS28-1 test was designed by AECL in Canada to determine the characteristics of the thermal hydraulic behavior in a fuel channel for a high fuel temperature and a low steam flow which might occur in some severe accident scenarios. The test procedure was divided into three stages: a steady state phase, a low power heat-up phase and a high power heat-up phase. This paper examines only the steady state phase where chemical reactions on the surface of the FES do not occur.

The experimental facility consisted of a test section of a 28-element fuel bundle including the calandria tube, a cooling water tank to simulate the moderator tank, a boiler to produce superheated steam, and a condenser (Fig. 1). The structure of the 28-element fuel bundle (Fig. 2, (a)) represented the Pickering-type CANDU fuel bundle. The test section was composed of three rings of fuel element simulators (FES) concentrically located inside the pressure tube (Fig. 2, (b)). Each FES consisted of Zr-4 cladding, with a 15.2 mm outside diameter (OD) and 14.4 mm inner diameter (ID), within which annular alumina pellets of 14.3 mm in OD and 6.1 mm in ID electrically insulated the cladding from a graphite rod heater. The length of the graphite rod heater simulating a decay power was 1800 mm. Twenty eight rod heaters were electrically powered, except for one failed heater (R1-1) which was located in the inner ring of the elements (Fig. 2, (a)).

In the steady state phase, 10 kW power was supplied to the heater. Electrical power was distributed at the ratio of 0.78 : 0.88 : 1.11 for the elements in the inner, middle and outer rings, respectively. The FES bundle was surrounded by a 2105 mm long section of an autoclaved Zr-2.5 Nb pressure tube which was mounted inside a 1780 mm long Zr-2 calandria tube (Fig. 2). The calandria tube section was submerged in the cooling tank of 1650 mm in length to a depth of 75 mm. The test section annulus had a gap between the pressure tube and the calandria tube, through which CO₂ gas of 6 l/min flowed to maintain the oxide layer on the outside of the pressure tube. Five space grids (Fig. 2, (b)) were evenly distributed along the axial direction in the test section. These can enhance the thermal mixing between the lower temperature steam and the higher temperature steam because the small holes, from 4 mm to 8 mm in diameter, actively generate an eddy motion.

The experiment was started by providing superheated steam (700 °C) at 1 bar into the test section at a flow rate of 10 g/s. Thermocouples were installed to measure the temperature of the steam, the FES, the pressure tube, the calandria tube and the water in the cooling tank. Thermocouples were installed mostly around the end part of the test section, from 1.1m to 1.7 m, to measure the temperature variation along the axial and radial directions. The uncertainties of the measurement devices are shown in Table 1.

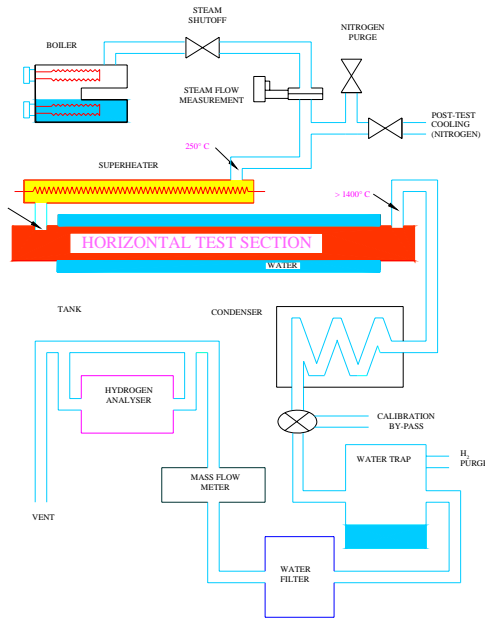


Fig. 1 Schematic diagram of the experimental facility

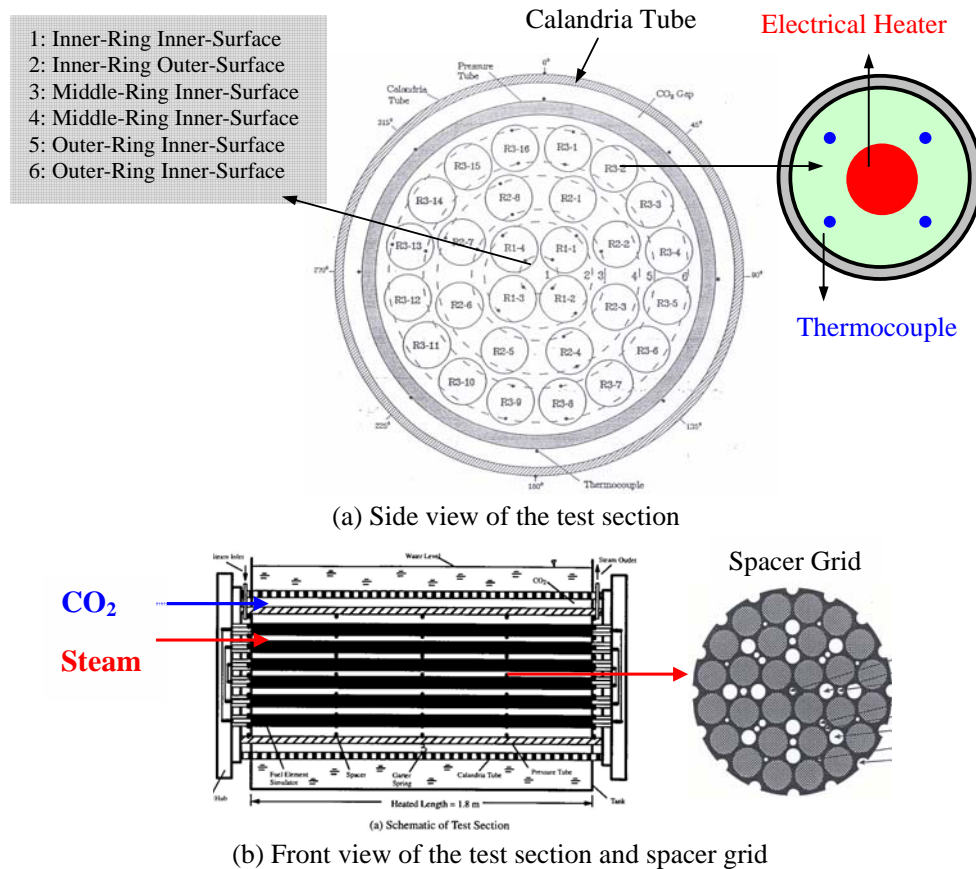


Fig. 2 Side view and front view of the test section

Table 1 Uncertainties of the Measurements

Measurement Variable	Uncertainty
Electric Power	$\pm 4.4\%$
Temperature up to 2000 °C	$\pm 1.2\%$
Steam Flow at 10 g/s	$\pm 2.0\%$
H2 Flow up to 0.75 mol/s	$\pm 1.1\%$
Pressure up to 500 kPa	$\pm 0.3\%$

The CS28-1 test in the steady state mainly measured the temperature of the steam, the inner/middle/outer FES, the pressure and the calandria tubes, and the water in the cooling tank. The heat balance in the CS28-1 test showed that the heat flux from the FES to the cooling tank by a radiation heat transfer was about $7.8 \text{ kW} \pm 1.3 \text{ kW}$ [7-10]. The steam temperature at the entrance region was 653°C and 553°C at TC63 and TC64, respectively (Fig.3). Steam temperatures at TC65, TC66 and TC67 in the outlet region were 697°C , 671°C and 685°C , respectively (Fig.3). The temperatures in the inner and middle FES were an almost constant value at around 700°C along the axial direction (Fig. 3), but the outer FES temperature was decreased from 683°C to 656°C (Fig. 3). The temperature of the pressure tube showed a slightly increasing temperature trend to about 500°C along the axial direction (Fig. 3). About 15 % of the heater power was estimated to be transferred by a convection heat transfer of steam and CO_2 [7-10]. There were large uncertainties in this estimate since only two thermocouples were installed in the cooling tank. Steam partly condenses at the unheated part of the FES before entering into the test section, causing a further uncertainty. Steam temperature difference of about 100°C was seen at the inlet when compared to a 26°C difference at the outlet (Fig. 3). The space grid may play a role in a thermal mixing between low and high temperature steam when the steam passes it. This temperature variation along the axial direction is different from that of a pure convection heat transfer [14-16]. The temperature of the pressure tube was slightly increased from 490°C to 510°C . This temperature variation is similar to a pure convection heat transfer because a radiation heat transfer is not as dominant as between the FESs and the pressure tube.

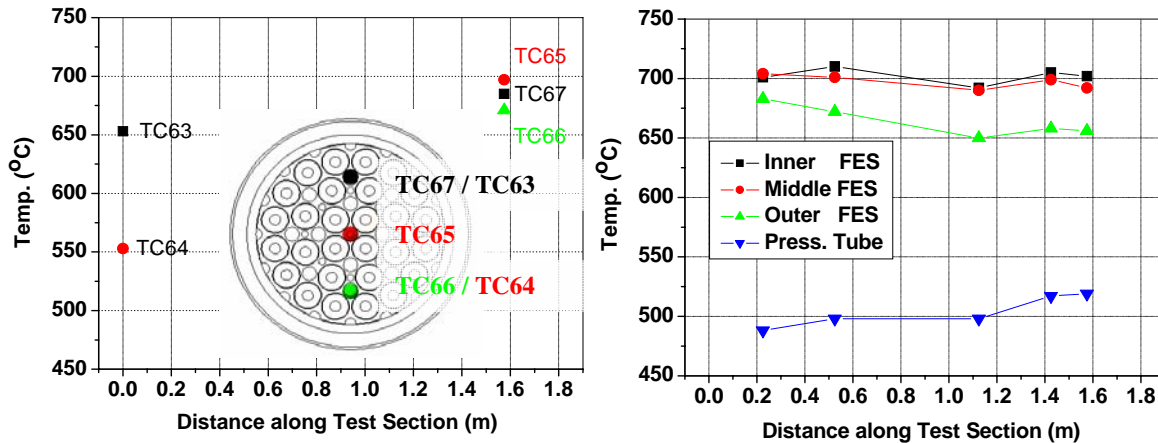


Fig. 3 Steam/FES/PT temperature along the axial direction

CFD Analysis

A full grid model of FES to the calandria tube simulating the test section (Fig. 4) was generated, because the non-uniform steam temperature of about a 100 °C difference at the inlet condition may have a large effect on the heat transfer phenomena in the fuel channel. And also, a spacer grid model with many small holes was implemented to simulate the thermal mixing between the high and low temperature steam when the steam passed it. A lot of mesh cells were required to resolve the complicated geometry and to produce a good quality grid model. The number of generated meshes in the grid model was 4,324,340 cells including 180 cells along the axial direction.

As for the boundary conditions, a heat source condition simulating an electric heater power of 10 kW in the CFD analysis was given according to the power ratio. The inlet boundary condition [17] was set separately at the entrance region for the steam and the CO₂ in the test section. The assumed temperature distribution at the inlet region is given in Figure 5. A uniform inlet velocity for the steam and the CO₂ was assumed. The outlet pressure boundary condition [17], the Neumann condition, was set at the outlet region for the steam and the CO₂ in the test section. The temperature dependent properties of the heat structures of zirconium, alumina and graphite in the test section were used for the CFD input [5-7,18-22]. The boundary conditions for this CFD analysis are summarized in Table 2.

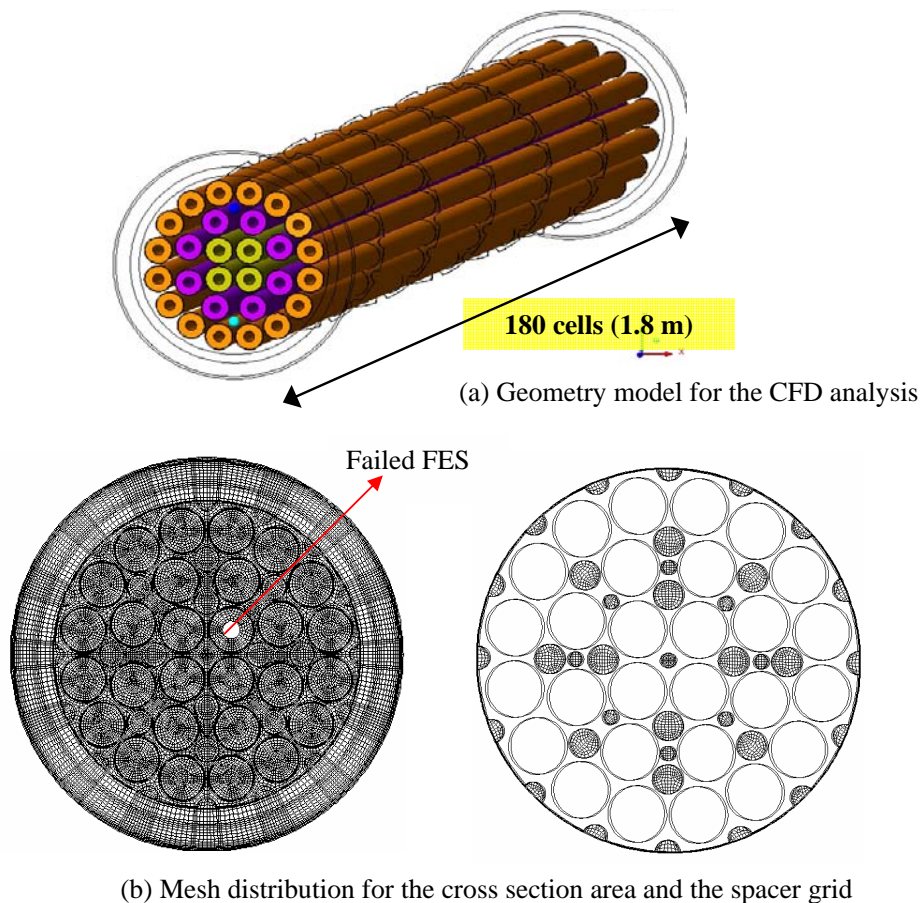


Fig. 4 Grid model for the CFD Analysis

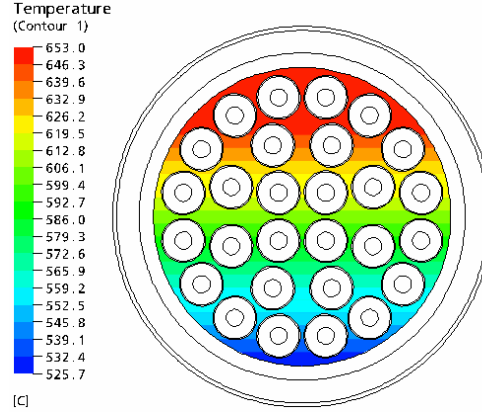


Fig. 5 Steam inlet temp. distribution in the CFD Analysis

Table 2 The Values for the Boundary Conditions

Heat Source Condition		
Inner FES	853.7 W	
Intermediate FES	2566.6 W	
Outer FES	6421.7 W	
Inlet Boundary Condition		
Steam (Fuel Channel)	11.72 m/s	653 °C ~ 553 °C
CO ₂ (Annulus Gas)	0.033 m/s	20 °C
Outlet Boundary Condition		
Steam (Fuel Channel)	0 Pa (reference value)	
CO2 (Annulus Gas)	0 Pa (reference value)	
Emissivity Value for Radiation Calculation [5-8,18-21]		
FES Outer Surface	0.8	
PT Inner Surface	0.8	
PT Outer Surface	0.8	
CT Inner Surface	0.34	
Gas Absorption Coefficient for Radiation Calculation [18]		
Steam & CO ₂	Plank-mean	

Fluid flow and heat transfer phenomena in the high temperature fuel channel were treated as a compressible flow, a highly turbulent flow, and a conduction/convection/radiation heat transfer. The governing equations used in this calculation were the mass conservation, Navier-Stokes and total energy equations (Eq. (1)~(3)) with a coupled solver algorithm [17,23]. The standard k-ε turbulent model (Eq. (4)~(5)) was used for a calculation of the eddy viscosity [17]. The model for the radiation transport equation used in the CFD analysis was the discrete transfer model [17,18,24].

$$\frac{\partial \rho}{\partial t} + \nabla \cdot (\rho V) = 0 \quad (1)$$

$$\frac{\partial \rho V}{\partial t} + \nabla \cdot (\rho V \otimes V) = \nabla \cdot \left(-P \delta + \mu \left(\nabla V + (\nabla V)^T \right) \right) \quad (2)$$

$$\frac{\partial \rho h_{tot}}{\partial t} - \frac{\partial p}{\partial t} + \nabla \cdot (\rho V h_{tot}) = \nabla \cdot (\lambda \nabla T) + S_E \quad (3)$$

$$\frac{\partial}{\partial t}(\rho k) + \nabla \cdot (\rho V k) - \nabla \cdot \left[\left(\mu + \frac{\mu_T}{\sigma_k} \right) \nabla k \right] + P_k - \rho \varepsilon \quad (4)$$

$$\frac{\partial}{\partial t}(\rho \varepsilon) + \nabla \cdot (\rho V \varepsilon) - \nabla \cdot \left[\left(\mu + \frac{\mu_T}{\sigma_\varepsilon} \right) \nabla \varepsilon \right] = C_1 \frac{\varepsilon}{k} P - C_2 \rho \frac{\varepsilon}{k} \quad (5)$$

$$\frac{dI_v(r, s)}{ds} = -(K_{av} + K_{sv})I_v(r, s) + K_a I_b(v, T) \quad (6)$$

The result of the heat balance calculations and the temperatures in the steam, and the inner/middle/outer FES and the pressure tube during a steady state in the CFD calculation are shown in Table 2 and Figures 6~10. About 81% of the heat source given by the user input was transferred into the cooling tank from the FES by a radiation and conduction heat transfer through CO₂. About a 100°C difference of the steam temperature was found at the inlet region, but only a difference of 30 °C, 670~700 °C, at the outlet (Fig. 6). The inner/middle/outer FES temperature along the axial direction was increased from 670 °C to 703 °C, 680 °C to 705 °C, and 610 °C to 662 °C, respectively (Fig. 7~9). The temperature of the inner and middle FES showed an almost constant value of about 700 °C along the axial direction (Fig. 7~8), but the outer FES temperature was decreased from 683 °C to 656 °C (Fig. 9). Temperature of the pressure tube showed a difference of 95 °C (475~560 °C), but only a 8 °C (552~560 °C) difference was found at the inlet (Fig. 10).

The steam temperature (Fig. 6) at some locations in the test results (TC63~TC67) when compared with those of the CFD showed a higher temperature at the upper region (TC65) in the CFD results and a lower temperature at the center and bottom regions within 5°C. This difference is small when considering the uncertainty of the test. The inner/middle/outer FES temperature distributions of the CFD results (Fig. 7~9) showed a small overestimated value of about 30°C at the entrance region, but a good agreement at the outlet region. The trend of the calculated FES temperatures showed a continuous increase along the axial direction. The difference between the CFD results and the test data at the entrance region may be due to an error in radiation heat transfer calculation [24], or to a wrong assumption of the inlet temperature distribution in the CFD analysis. The comparison of the outer FES temperature at the entrance region (Fig. 9) showed that a linearly assumed inlet temperature distribution may not sufficiently represent the test phenomena, because a big difference of about 70°C only occurred at the lower right FES. This means that high temperature steam discharged from the top region of pressure tube may arrive at the lower right region through a pathway of the center from the top to the bottom. However, comparison results of the pressure tube also indicated that the discrete transfer model for a radiation heat transfer calculation has an error, because a temperature difference of about 30 °C at the outlet region is large when compared with the comparison for the steam and FES temperature. A verification of the discrete transfer model [24] and CFD sensitivity calculation by using another assumed temperature distribution for the inlet should be performed.

Table 3 Results of the Heat Balance in CFD Calculation

Heat Source (FES)	Convection H. T (Steam)	Radiation & Conduction H. T (Calandria Tube Outer Surface)
9.84 kW	1.48 kW	8.01 kW

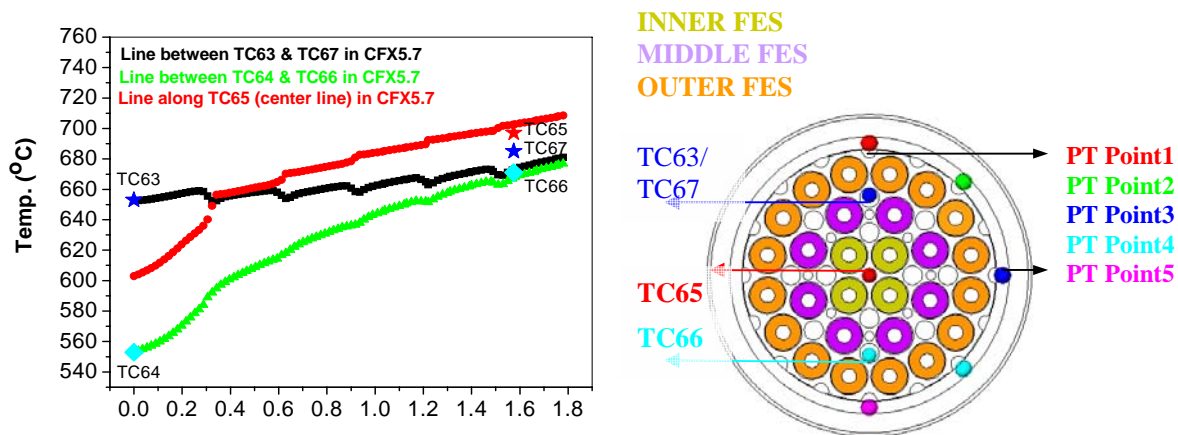


Fig. 6 Comparison Results of the Steam Temperature

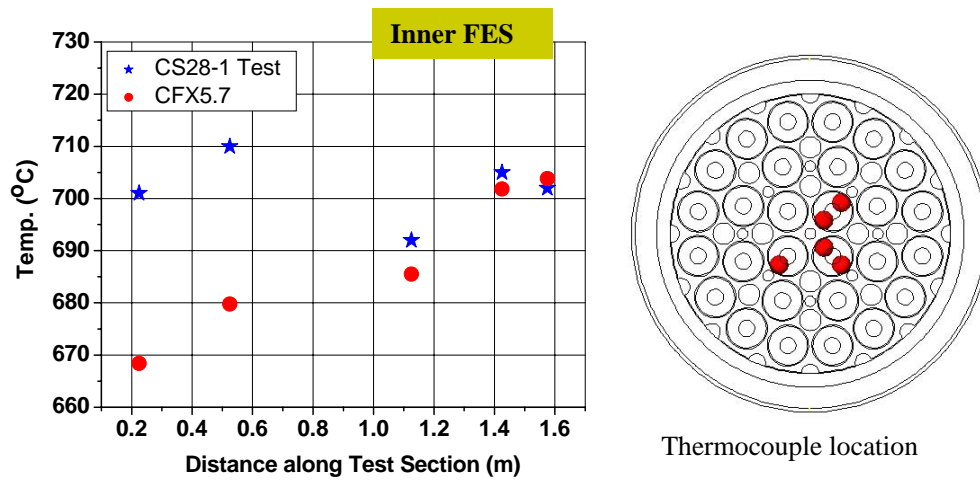


Fig. 7 Comparison Results of the Inner FES Temp.

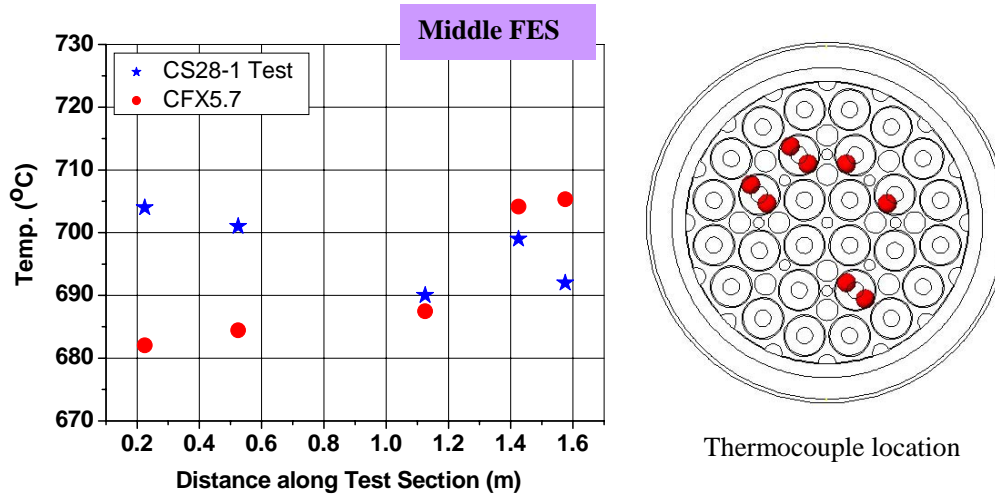


Fig. 8 Comparison Results of the Middle FES Temp.

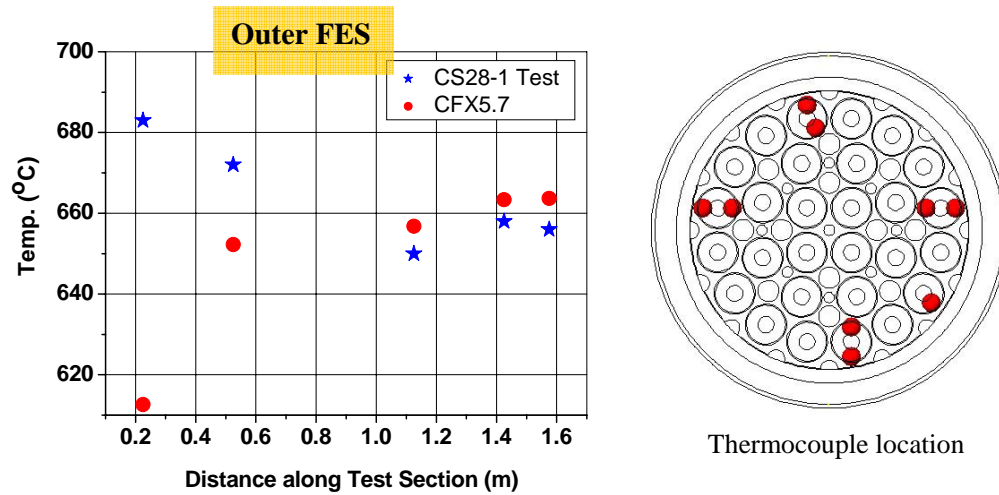


Fig. 9 Comparison Results of the Outer FES Temperature

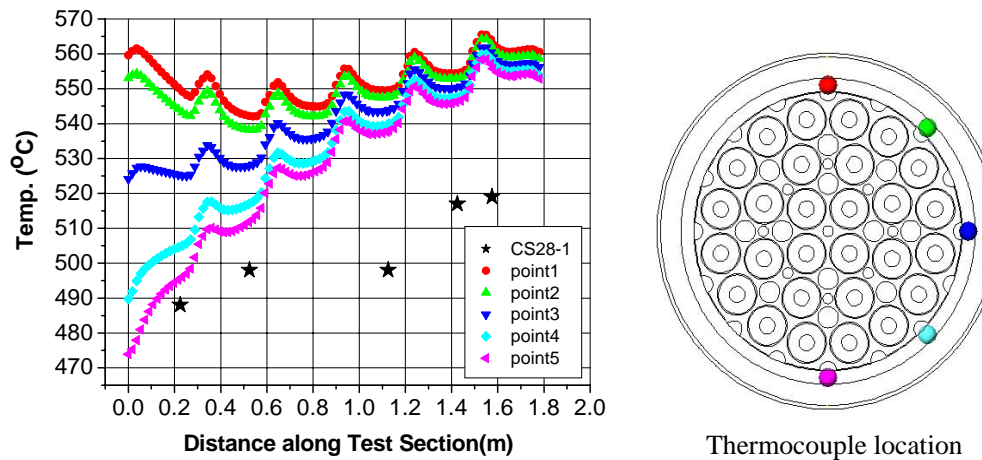


Fig. 10 Comparison Results of the Pressure Tube Temperature

Conclusions

The CFD benchmark calculation for the post-blowdown test in a CANDU fuel channel was performed to assist in the development of a new safety analysis strategy and to develop a CFD analysis methodology which can be used in the safety analysis of CANDU. The CFD results showed good agreement for the trend of the test results as a whole. However, the CFD results overestimated the temperature of the inner/middle/outer FES at the entrance region and the pressure tube temperature at the outlet region. This may be due to the fact that the enthalpy increase of the CO₂ due to its absorbing thermal photons is overestimated. To resolve these problems, a proper gas absorption coefficient for CO₂ should be adopted and a sensitivity CFD calculation should be performed.

Acknowledgements

This work was financially supported for the nuclear R&D program from the Ministry of Science and Technology of Korea. The authors are sincerely grateful for the financial support.

References

1. KOPEC, Wolsong 2, 3, 4 Final Safety Analysis Report, **ch.15** (2001).
2. B-J Min et al, *Development of Safety Assessment System and Safety Issues Relevant Technology for CANDU Reactors*, Research Report, KAERI/RR-2500/2004, KAERI (2004).
3. B. W. Rhee, H. S. Kang and B-J Min, "Improvement of Post-blowdown Fuel Channel analysisModel of CANDU 35% RIH Break LOCA without ECC," *Proc. of ICAPP '04*, Pittsburg, USA, June 13-17 (2004).
4. H. S. Lim, K.M. Lee, and et al., "Validation of CATHENA against the CS28-1 High Temperature Experiment Under an Impaired Cooling Condition", *Ann. Nucl. Energy*, **22**, No.9, pp.593-600 (1995).
5. M. H. Bayoumi and W. C. Mur, "Post-Test Simulation and Analysis of the Second Full Scale CHAN 28-Element Experiment (Validation of CHAN-II (MOD 6) Against Experiments), *Proc. of the 16th Annual CNS Conference*, Saskatoon, Canada (1995).
6. M. H. Bayoumi, W. C. Mur and P. S. Kundurpi, "Post-Test Simulation of the First CHAN 28-Element Experiment (Verfication of CHAN-II MOD 6 Against Experiment), *Proc. of the 4th International Conference on Simulation Methods in Nuclear Engineering*, Montreal, Canada (1993).
7. Q. M. Lei and T. M. Goodman, "Validation of Radiation Heat Transfer in CATHENA", *Proc. of the 5th International Conference on Simulation Methods in Nuclear Engineering*, Montreal, Canada (1996).
8. Q. M. Lei, D. B. Sanderson, K. A. Haugen and H. E. Rosinger, "Post-Test Analysis of the 28-Element High-Temperature Thermal-Chemical Experiment CS28-1", *Proce. of the 4th International Conference on Simulation Methods in Nuclear Engineering*, Montreal, Canada (1993).
9. D. B. Sanderson, K. A. Haugen, R. G. Moyer and H. E. Rosinger, "Out-of-Pile Fuel Channel Experiments for Severe Accidents Conditions", *Proc. of the ANS International Topical Meeting on Safety of Thermal Reactors*, Portland, OR, pp.92-100 (1991).
10. T. Nitheanandan, "CHAN 28-Element Fuel-Channel Thermal-Chemical Expeiments", *AECL Presentation Material in the 4th JRDC Meeting*, KAERI, Taejon, Korea, May 19-20 (2005).
11. H. S. Kang, B. W. Rhee and B-J Min, "CFD Analysis against the steady state experiment for Post-blowdown Phenomena in the CANDU fuel channel", *Proc. of the '04 KNS Autumn Conf.*, Yongpyong, Korea, Oct. 27-28 (2004).
12. H. S. Kang, B. W. Rhee and B-J Min, "CFD Analysis for Experiment of Single Channel Post-Blowdown", *Proc. of the '05 KNS Spring Conf.*, Jeju, Korea, May 26-27 (2005).
13. H. S. Kang, B. W. Rhee and J-Hwan Park, "CFD Analysis for a Natural Convection in the Annulus Gap Under Post-blowdown", *Proc. of the '05 KNS Autumn Conf.*, Busan, Korea, Oct. 28-29 (2005).
14. T.H.Kuehn and R.J.Goldstein, "Correlating Equations for Natural Convection Heat Transfer Between Horizontal Circular Cylinder", *Int. J. Heat Mass Transfer*, **19**, pp.1127-1134 (1976)
15. J. T. Rogers and S. S. Goindi, "Effect of Gas Flow in the Insulating Annulus on Fuel Channel Temperatures in a Severe Accident in a CANDU Reactor", *Proc. of the 7th Annual CNS Conference*, pp.163-167 (1986).

16. M. Perlmutter and R. Siegel, "Heat Transfer by Combined Forced Convection and Thermal Radiation in a Heated Tube", *Journal of Heat Transfer*, **C84**, pp.301-311 (1962).
17. ANSYS, Inc., CFX5.7 Manual (2004).
18. Michael F. Modest, *Radiative Heat Transfer*, **2nd ed.**, ch.10, McGraw-Hill, New York (1993).
19. V. F. Urbanic and T. R. Heidrick, "High-Temperature Oxidation of Zircaloy-2 and Zircaloy-4 in Steam", *Journal of Nuclear Material*, **75**, pp.251-261 (1978).
20. D. H. Bradhurst and P. M. Heuer, "The Temperature Dependence of the In-Reactor Oxidation of Zirconium Alloys in Moist CO₂ Atmospheres from 573-868K", *Journal of Nuclear Material*, **96**, pp.196-204 (1981).
21. P. M. Mathew, M. Krause, M. Dean and M. H. Schankula, "Emittance of Zircaloy-4 Sheath at High Temperatures in Argon and Steam Atmospheres", *Proc. of the 10th Annual CNS Conference*, Ottawa, ON (1989).
22. Bejan, *Convection Heat Transfer* **2nd ed.**, Wiley Inter. Science (1995).
23. F. R. Menter, P. F. Galpin and et al, "CFD Simulation of Aerodynamic Flow with a Pressure-based Method", *Proc. of the 24th International Congress of the Aeronautical Science*, Yokohama, Japan (2004).
24. P. J. Coelho and M. G. Carvalho, "A Conservative Formulation of the Discrete Transfer Method", *Journal of Heat Transfer*, **119**, pp.118-128 (1997).